Ground and excited states of linked and fused zinc porphyrin dimers: Symmetry adapted cluster (SAC)—configuration interaction (CI) study

T. Miyahara, H. Nakatsuji,[a] and J. Hasegawa
Department of Synthetic Chemistry and Biological Chemistry, Graduate School of Engineering, Kyoto University, Sakyo-ku, Kyoto, 606-8501, Japan

A. Osuka, N. Aratani, and A. Tsuda
Department of Chemistry, Graduate School of Science, Kyoto University, Sakyo-ku, Kyoto 606-8502, Japan

(Received 6 August 2002; accepted 24 September 2002)

The symmetry adapted cluster (SAC)/SAC-configuration interaction method was applied to calculate the ground and excited states of zinc porphyrin monomers (without and with phenyl groups, ZnP and ZnPPh, respectively) and meso–meso linked (Zn_2PMM) and doubly fused (Zn_2PDF) zinc porphyrin dimers. Various features of the absorption spectra are studied, clarified, and assigned theoretically. The calculated electronic spectrum of ZnPPh, in comparison with that of ZnP, showed that the phenyl groups affect the spectrum in both the peak positions and intensities. In the dimers, Zn_2PMM and Zn_2PDF, the interactions of the monomer's four-orbitals result in an eight-orbital model of the dimers, which plays an important role in the interpretation of the excited states observed in the spectra. In Zn_2PMM, the interaction is smaller and each peak in the split Soret (BI and BII) bands consists of two peaks, in contrast to the prediction based on Kasha's exciton rule. In Zn_2PDF, the interaction between the two monomer units is so strong that the small highest occupied molecular orbital–lowest unoccupied molecular orbital gap causes the red-shifted Q (1.16 eV) and BI (2.13 eV) bands. In addition, the excitations out of the eight orbitals appear in the low-energy region of the spectrum, which is very different from the case of the monomer. A comprehensive and pictorial analysis is given for the excited states of the dimers in comparison with those of the monomer. © *2002 American Institute of Physics.*
[DOI: 10.1063/1.1521763]

I. INTRODUCTION

Recently, various linker- or sandwich-type multiporphyrin arrays have been extensively studied.[1] Several directly linked and fused porphyrin arrays were synthesized and their properties were investigated by Osuka *et al.*[2] These compounds may play a role in the light-harvesting system in photosynthesis,[3] where efficient electron and energy transfer must occur over a long distance. π-Conjugated molecules with a small highest occupied molecular orbital–lowest unoccupied molecular orbital (HOMO–LUMO) gap have also been studied with regard to their potential use as molecular wires in molecular-scale electronics and nanotechnological devices.[4] Monodisperse linear π-conjugated molecules can reach a length of 10 nm. The porphyrins are some of the most attractive molecular units, since they are rigid, have planar geometries, are highly stable, and show intense electronic absorptions and a small HOMO–LUMO gaps. Studies on polymeric porphyrins have led to the possibility of an artificial light-harvesting system and also improve our understanding of the complicated mechanism in photosynthesis.

Previously, we reported the ground and excited states of many porphyrin systems[5] using the SAC (symmetry adapted cluster) theory[6] for the ground state and the SAC-CI theory[7] for the excited state. The SAC/SAC-CI method has been established as a powerful quantum mechanical tool that can be applied to various ground and excited states from singlet, triplet, ionized and electron-attached states of molecules to even septet spin multiplicities.[8,9] It has been shown to be necessary to include a large amount of electron correlations for a reliable understanding of the electronic structures of the ground and excited states of various porphyrins.[5]

We report here the SAC/SAC-CI studies on the ground and excited states of two zinc porphyrin dimers: One is the meso–meso linked dimer Zn_2PMM and the other is doubly fused dimer Zn_2PDF as shown in (2) and (3), respectively, of Fig. 1. In Zn_2PMM, two porphyrins are connected at meso–carbon in perpendicular orientation to each other. The Soret band of Zn_2PMM splits into two intense absorption peaks.[2(c)] The higher-energy absorption peak (which we call the BII band) in the Soret region does not shift and has almost the same energy as the Soret band of the monomer. The lower-energy absorption peak (BI band), on the other hand, shifts by about 0.2 eV in lower side. The Q band of the meso–meso dimer is slightly red-shifted and has a stronger intensity than that of the monomer.

In the doubly fused dimer, the two porphyrins are in the same plane, and have one meso–meso and two β-β linkages. The Soret band of the doubly fused dimer is split into two intense absorption peaks, as in the meso–meso dimer.[2(d)] The higher-energy absorption peak (BII band) in the Soret region does not shift and is at an energy region close to that of the

[a]Author to whom correspondence should be addressed. Fax: +81-75-753-5910. Electronic mail: hiroshi@sbchem.kyoto-u.ac.jp

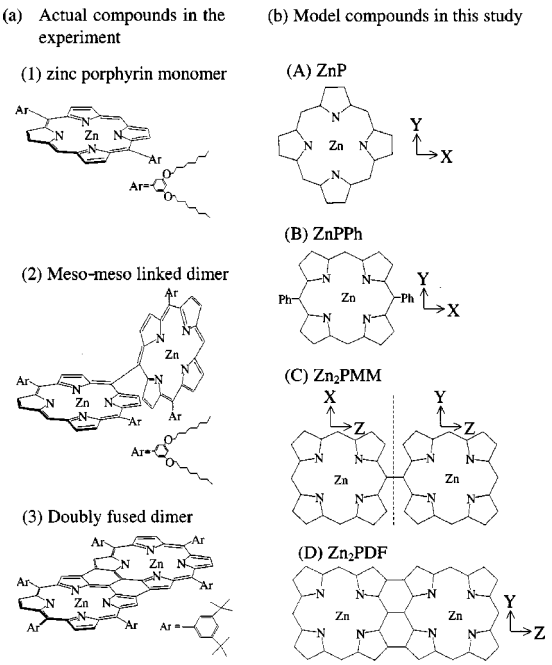

FIG. 1. Zn porphyrin compounds: (a) Actual compounds in the experiment: (1) zinc porphyrin monomer, (2) meso–meso linked dimer and (3) doubly fused dimer. (b) Model compounds used in this study: (A) ZnP and (B) ZnPPh, a model compound of (1), (C) Zn_2PMM, a model compound of (2), and (D) Zn_2PDF, a model compound of (3).

monomer. However, the lower peak (BI band) shifts by about 0.8 eV and appears in the region of the Q band of the monomer. The Q band of the doubly fused dimer also shifts by 1.1 eV and has a stronger intensity than that of the monomer.

In Sec. II, we describe the details of the calculations: The model geometry, basis sets, computational program, computational conditions and so on. In Sec. III, we study the molecular orbital (MO) pictures of the electronic structures of the two zinc porphyrin dimers in comparison with those of the zinc porphyrin monomer. In Sec. IV, we report the excited states of the zinc porphyrin monomer without phenyl groups, in comparison with those of magnesium porphin (MgP) calculated previously.[5(a)] In Sec. V, we report the excited states of the zinc porphyrin monomer with phenyl groups, and show the effect of phenyl groups. In Sec. VI, we report the excited states of the meso–meso linked dimer, and explain the cause of the splitting of the Soret band. In Sec. VII, we report the excited states of the doubly fused dimer, and explain the cause of the red-shifted Q and BI bands and the presence of many complicated features in the excitation spectrum.

II. COMPUTATIONAL DETAILS

We performed four different model calculations (A)–(D). Model (A) is a zinc porphyrin monomer without porphyrin side chains, and is referred to as ZnP. Model (B) is a zinc porphyrin monomer with phenyl groups as porphyrin side chains, and is referred to as ZnPPh. The phenyl group is perpendicular to the porphyrin ring. Model (C) is a meso–meso linked zinc porphyrin dimer, and is referred to as Zn_2PMM. The angle between the two porphyrins is fixed at 90 degrees. Model (D) is a doubly fused zinc porphyrin dimer, and is referred to as Zn_2PDF. These compounds are shown in Fig. 1.

In model (A), ZnP ($ZnC_{20}N_4H_{12}$) has D_{4h} symmetry and consists of 37 atoms and 190 electrons. In model (B), ZnPPh ($ZnC_{32}N_4H_{20}$) has D_{2h} symmetry and consists of 57 atoms and 270 electrons. In model (C), Zn_2PMM ($Zn_2C_{40}N_8H_{22}$) has D_{2d} symmetry and consists of 72 atoms and 378 electrons. In model (D), Zn_2PDF ($Zn_2C_{40}N_8H_{18}$) has D_{2h} symmetry and consists of 68 atoms and 374 electrons. The geometries of these model compounds were optimized by the DFT[10] method with B3LYP potential.[11]

The basis set is of valence double-ζ quality for all calculations. For the Zn atom, we use Huzinaga's (5333/532/5)/[53321/5311/41] set,[12] for the C and N atoms we use the (63/5)/[621/41] set,[12] and for the H atom we use the (4)/[4] set.[13] We do not add polarization functions: in our previous calculations,[5(a)] we found that the polarization functions are not essential for the reproduction of the absorption spectra of porphyrin compounds.

The Hartree–Fock (HF) self-consistent field (SCF) calculations were performed using GAUSSIAN 98 suite of programs.[14] The HF SCF orbitals consist of 95 occupied and 162 unoccupied MOs in model (A), 135 occupied and 238 unoccupied MOs in model (B), 189 occupied and 323 unoccupied MOs in model (C), and 187 occupied and 321 unoccupied MOs in model (D). The SAC/SAC-CI calculations were carried out using the program SAC-CI96.[15] Since it was computationally demanding to include all of the valence MOs, except in model (A), we included MOs with orbital energies of -1.2 to $+1.3$ a.u. in the active space. In model (A), the active space is comprised of 62 higher occupied MOs and all of the unoccupied MOs (total 224 MOs), while the core orbitals ($1s$ orbitals of C and N atoms; $1s$, $2s$, $3s$, $2p$, and $3p$ orbitals of Zn) were treated as frozen MOs. The active space consists of 86 higher occupied and 196 lower unoccupied MOs (total 282 MOs) in model (B), 115 higher occupied and 258 lower unoccupied MOs (total 373 MOs) in model (C), and 113 higher occupied and 251 lower unoccupied MOs (total 364 MOs) in model (D). Perturbation selection was performed for the double excitation operators.[5(e),16] We used an energy threshold of 1×10^{-5} a.u. for the ground state of all four compounds. For the excited state, a threshold of 1×10^{-6} a.u. in calculations (A2) and (B) and 5×10^{-7} a.u. in calculations (A1), (C), and (D) were used.

III. MOLECULAR ORBITALS OF THE MONOMERS AND DIMERS

The energies and characters of the SCF-MOs in calculations (A)–(D) are shown in Table I.

In calculation (A), the SCF MOs of ZnP are very similar to those of magnesium porphin (MgP) reported previously.[5(a)] Figure 2 shows the shapes of the MOs of ZnP. The HOMO (a_{1u}), next-HOMO (a_{2u}) and degenerate LUMO are the so-called four-orbitals of Gouterman.[17] The MOs 90 and 93 are also very similar to those of MgP and the importance of these MOs will be discussed later. All of these MOs are delocalized over the porphyrin ring.

TABLE I. HF orbital energy and orbital character of (A) ZnP, (B) ZnPPh, (C) Zn_2PMM, and (D) Zn_2PDF.

(A) ZnP			(B) ZnPPh			(C) Zn_2PMM			(D) Zn_2PDF		
MO number	Orbital energy (eV)	Nature[a]	MO number	Orbital energy (eV)	Nature[a]	MO number	Orbital energy (eV)	Nature[a]	MO number	Orbital energy (eV)	Nature[a]
Occupied orbitals											
88, 89	−10.26	π	124	−10.22	π	174	−10.37	π	172	−10.95	σ, Zn d
						175, 176	−10.24	π	173	−10.74	σ, Zn d
			125	−10.12	π	177	−10.16	π	174	−10.72	π
									175	−10.14	π
90	−9.941	π	126	−9.859	π	178, 179	−9.932	π	176	−9.999	π
			127	−9.470	π, Ph				177	−9.896	π
91, 92	−9.514	π	128	−9.456	π	180, 181	−9.513	π	178	−9.750	π
									179	−9.739	π
			129	−9.416	π	182, 183	−9.499	π	180	−9.525	π
									181	−9.523	π
			130	−9.291	Ph						
			131	−9.283	Ph						
			132	−9.279	Ph						
93	−9.458	π	133	−9.256	π, Ph	184	−9.479	π	182	−8.578	π
						185	−9.396	π	183	−8.456	π
94	−6.712	π	134	−6.621	π	186, 187	−6.733	π	184	−7.553	π
									185	−6.763	π
95	−6.369	π	135	−6.322	π	188	−6.547	π	186	−6.038	π
						189	−6.199	π	187	−5.932	π
Unoccupied orbitals											
96, 97	0.07891	π	136	0.08544	π	190	−0.1124	π	188	−1.213	π
						191, 192	0.03238	π	189	−0.1918	π
			137	0.1086	π	193	0.2683	π	190	0.3393	π
									191	0.8406	π
98	2.784	π	138	2.803	π	194, 195	2.745	π	192	2.044	π
			139	3.228	Ph						
			140	3.231	Ph						
			141	3.233	Ph						
			142	3.296	Ph						
99	3.849	Zn p_z	143	3.875	Zn p_z	196, 197	3.788	Zn p_z	193	3.767	Zn p_z
									194	3.858	Zn p_z
100	4.090	Zn s	144	4.030	Zn s	198	3.920	Zn s	195	4.018	Zn s
						199	4.014	Zn s	196	4.026	Zn s

[a]π is porphyrin π nature, Ph is π nature of phenyl group.

In calculation (B), the SCF MOs of ZnPPh are similar to those of ZnP as shown in Fig. 3. Porphyrin–phenyl interaction in ZnPPh is observed in some MOs. The HOMO, next-HOMO and MO 90 of ZnP are almost the same as those in ZnPPh. The LUMO and next-LUMO are not degenerate, in contrast to those in ZnP, due to the phenyl-group porphyrin side-chains, but the orbital energies of the LUMO and next-LUMO are very close to each other, as seen from Table I. The MOs 130 to 132 and 139 to 142 are localized on the phenyl groups. They are the π orbitals of the phenyl group and do not mix with the porphyrin π orbitals. In MOs 127 and 133, the π nature of the phenyl groups mixes with the porphyrin π nature, as shown in Fig. 3. The phenyl groups do not have an important effect on the energies and the shapes of the orbitals, since the porphyrin and phenyl groups are perpendicular to each other and interact only slightly.

Figure 4 shows the SCF MOs and orbital energies of Zn_2PMM of calculation (C). The HOMO and next-HOMO of Zn_2PMM originate from the HOMO of ZnP, and are delocalized over two porphyrins. The energy gap between the HOMO and next-HOMO is about 0.35 eV. The MOs 186 and 187 originate from the next-HOMO of ZnP and are localized on each porphyrin. These MOs maintain the monomer character: their orbital energies degenerate and are the same as those of ZnP. Meso–meso interaction through the π-orbitals does not cause π orbital mixing as in the case of the next-HOMO of ZnP, since the π orbitals of the meso–carbon are perpendicular to each other. However, the interaction between the HOMOs of the monomers can be seen in Zn_2PMM. In this case, the π orbital of the α-carbon interacts with that of the other porphyrin, which is similar to a δ bond. A similar situation is seen in the unoccupied and other occupied orbitals. The LUMO and the MO 193 of Zn_2PMM are delocalized on the two porphyrins, since the monomer LUMOs interact through the α-carbon. On the other hand, the MOs 191 and 192 are localized on one porphyrin and degenerate each other, since the monomer LUMOs interact through the meso–carbon. The energy gap between the LUMO and the MO 193 is about 0.38 eV. The MOs 186 to 193, which we call hereafter ''eight-orbital,'' correspond to the Gouterman's four-orbital and play an important role in the low-lying excited states of the dimer. The energy gap between HOMO and LUMO of Zn_2PMM is smaller than that in the monomer by 0.36 eV, due to the splitting of the

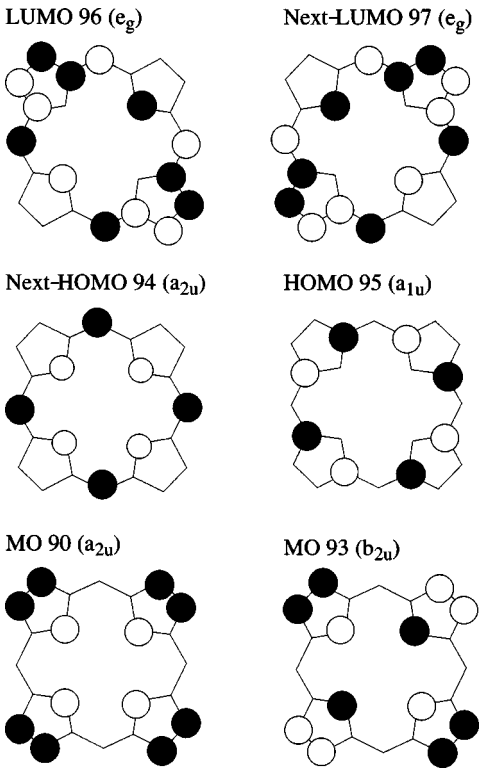

FIG. 2. SCF-MOs of (A) ZnP.

HOMO and next-HOMO, LUMO and MO 193.

The SCF MOs and orbital energies of Zn_2PDF are shown in Fig. 5. Since the two porphyrins are connected in the same plane, the interactions between the π orbitals are

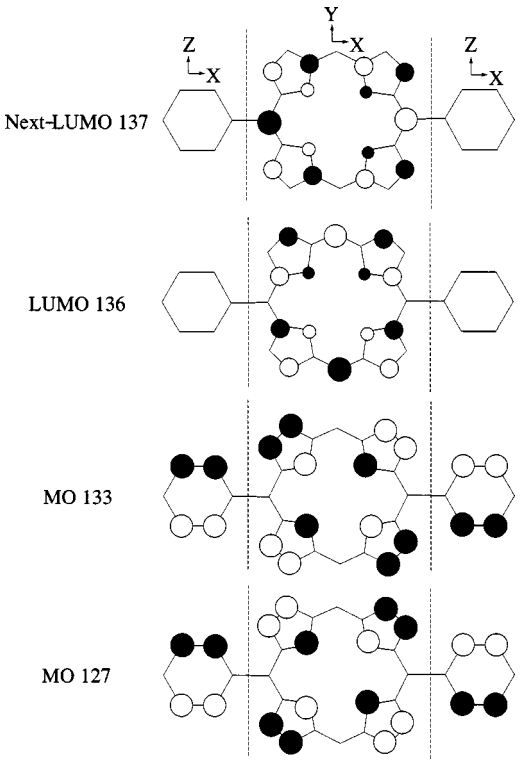

FIG. 3. Some SCF-MOs of (B) ZnPPh, which are different from those of ZnP. Note that the phenyl groups are rotated by 90 degrees for presentation.

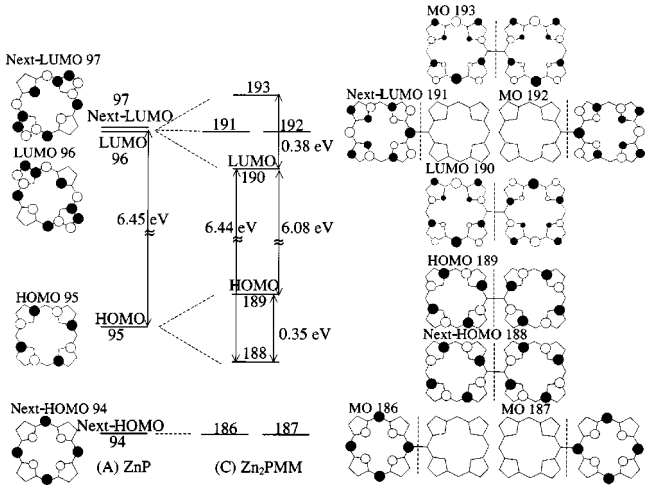

FIG. 4. SCF-MOs and orbital energies of (C) Zn_2PMM. Those of (A) ZnP are shown for comparison.

much stronger than those in Zn_2PMM. All of the MOs of Zn_2PDF are completely delocalized over the two porphyrins. The HOMO and the next-HOMO of Zn_2PDF are characterized as the anti-bonding combinations of, respectively, the next-HOMO and HOMO of the monomer. We note that the order is reversed by the strong ''fused'' dimerization. In contrast to Zn_2PMM, the interaction between the monomer MOs is greater for the MOs with amplitude at the meso- and β-carbons, since the monomers are directly connected at meso- and β-positions, which characterizes the orbital energy splitting caused by the dimerization. This is a cause, as

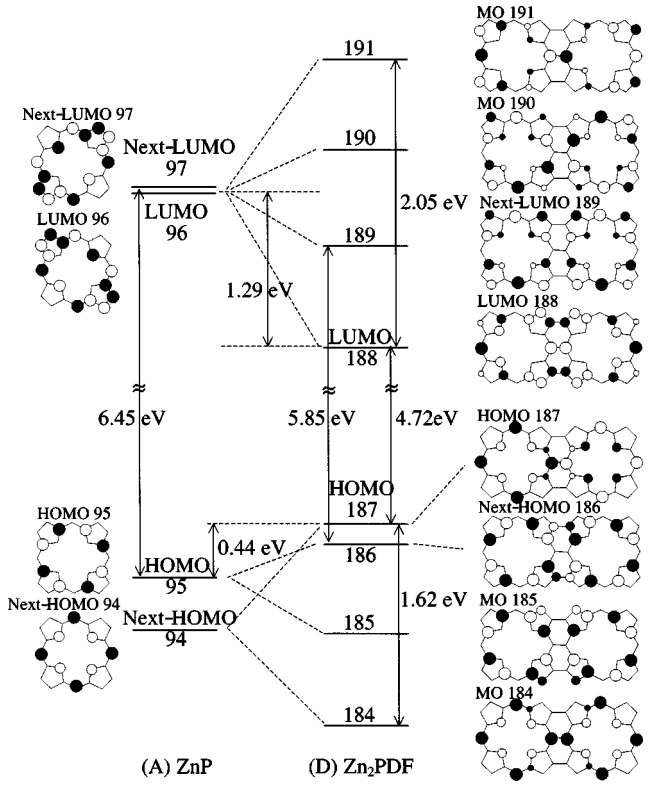

FIG. 5. SCF-MOs and orbital energies of (D) Zn_2PDF. Those of (A) ZnP are shown for comparison.

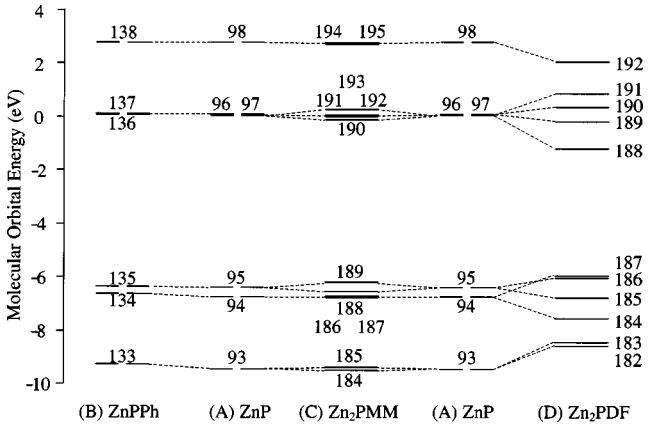

FIG. 6. The molecular orbital energies of (A) ZnP, (B) ZnPPh, (C) Zn_2PMM, and (D) Zn_2PDF.

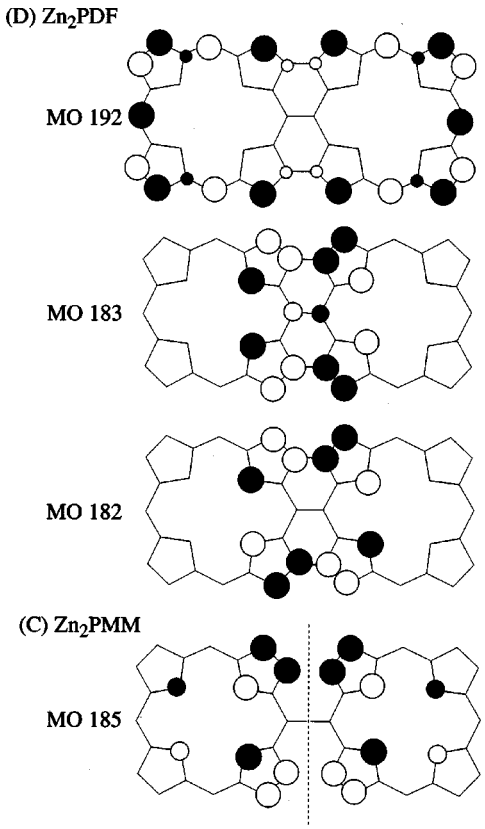

FIG. 7. SCF-MOs 182, 183, and 192 of (D) Zn_2PDF and SCF-MO 185 of (C) Zn_2PMM.

stated above, of the reversed order in the character between the HOMO and next-HOMO in Zn_2PDF: A large interaction at the meso-position between the next-HOMO of the monomers causes the large energy splitting of 1.62 eV between HOMO and MO 184 of Zn_2PDF, which raises the energy level of the anti-bonding combination to HOMO of the dimer. Similarly, since the LUMO and MO 191 have a large coefficient at the meso–carbon, the energy gap between LUMO and MO 191 is greater than that between next-LUMO and MO 190. The orbital energy of LUMO is lower than that of ZnP by 1.29 eV. The energy gap between HOMO and LUMO is 4.72 eV, which is much smaller than those in ZnP (6.45 eV) and Zn_2PMM (6.08 eV).

Figure 6 shows a MO energy diagram near the HOMO–LUMO level for ZnP, ZnPPh, Zn_2PMM, and Zn_2PDF. The orbital energies of ZnPPh are almost the same as those of ZnP. For Zn_2PMM, a slight upper shift and lower shift of about 0.2 eV, due to dimerization, can be seen. However, in Zn_2PDF, the orbital energies of the eight-orbital and also the MOs 182, 183, and 192 are significantly rearranged. The orbital energies of the MOs 182 and 183 are higher (by 0.9 eV) and that of the MO 192 is lower (by 0.74 eV) than those of the other compounds. Therefore, in Zn_2PDF, these MOs that are out of the eight-orbital are expected to play an important role in the excited states around the Soret band regions.

Figure 7 shows the shapes of the MOs 182, 183, and 192 of Zn_2PDF. MOs 182 and 183 are localized at the inner four pyrrole rings. These MOs have a large coefficient at the β-carbon. The interactions between porphyrins of these MOs are large, since the two porphyrins are connected by covalent bonds at their β-carbons. The orbital energies of these MOs with antibonding interaction at the β-β bond are higher than those in the other compounds. In Zn_2PMM, the MO 185 has a large coefficient at the β-carbon, but the interaction between porphyrins in this MO is slight, as seen in Fig. 7, since the two porphyrins have an orthogonal geometry. Similarly, the MO 192 has a coefficient at the β-carbon. The orbital energy of this MO with bonding interaction at the β-β bond is lower than those in the other calculations.

IV. EXCITED STATES OF ZnP

Figure 8 shows the SAC-CI theoretical spectrum for ZnP, in comparison with the experimental spectrum for ZnPPh measured in THF by Osuka *et al.*[2(c)] Table II summarizes the SAC-CI and SECI results for the optically allowed states. The main configurations, characters, excitation energies and oscillator strengths are shown. The results obtained by SAC-CI are similar to those for Mg porphin in a previous calculation.[5(a)]

The Q band (2.28 eV, 543 nm) is assigned to the $1\,^1E_u$ state calculated at 1.84 eV. The intensity is weak in accordance with the weakness of the observed peak. The main configuration consists of excitations within the four-orbital. The Q band has a small intensity, since the weights of the two main configurations, $1a_{1u}-5e_g$ and $5a_{2u}-5e_g$, are almost equal.[5(c)]

The B band (3.00 eV, 413 nm) is assigned to the $2\,^1E_u$ state calculated at 3.50 eV. The $2\,^1E_u$ state has a strong intensity and reproduces the strong sharp peak observed. The main configuration consists of not only the excitations within the four-orbital but also the excitation from $4a_{2u}$, MO 90 in Fig. 2, which has been established already as a common feature of the porphyrin compounds.[5(a),18] The Q–B separation is calculated to be larger than the experimental value, a common feature of the SAC-CI results for porphyrins.

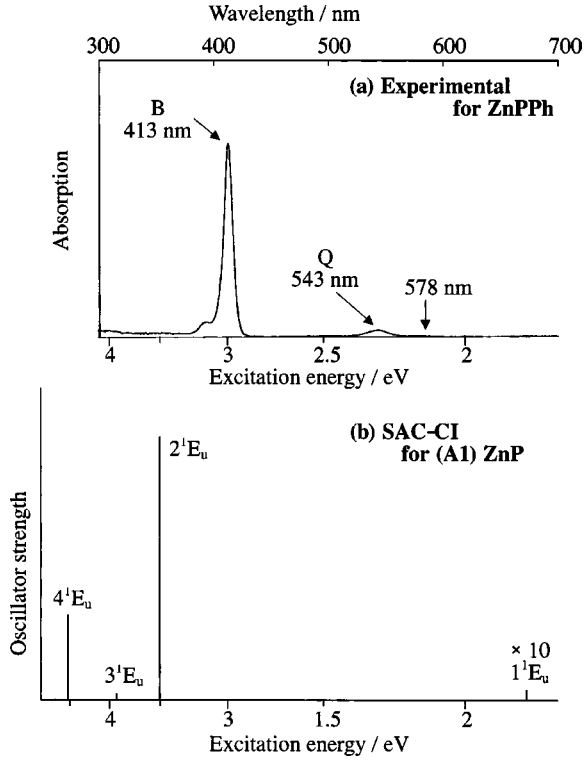

FIG. 8. (a) Experimental spectrum of zinc porphyrin monomer [2c], and (b) the SAC-CI theoretical spectrum for (A1) ZnP.

V. THE EFFECT OF PHENYL GROUPS

Figure 9 shows the SAC-CI theoretical spectrum for ZnPPh, in comparison with the experimental spectrum for ZnPPh measured in THF by Osuka *et al.*[2(c)] The SAC-CI theoretical spectrum for ZnP (A2), using the same computational condition as that for ZnPPh, is also shown for comparison. Tables III and IV summarize the SAC-CI and SECI results for the optically allowed states of ZnPPh and ZnP (A2), respectively. The main configurations, characters, excitation energies and oscillator strengths are shown.

The theoretical peaks of ZnP (A2), which has D_{4h} symmetry, are split into two peaks in the theoretical spectrum of ZnPPh (B), which has D_{2h} symmetry.

The Q band (2.28 eV, 543 nm) is assigned to the $1\,^1B_{2u}$ state calculated at 2.00 eV. In the energy region lower than the Q band, a peak observed at 578 nm (2.14 eV) is assigned to the $1\,^1B_{3u}$ state calculated at 1.98 eV. The oscillator strength of the $1\,^1B_{3u}$ state is smaller than that of the $1\,^1B_{2u}$ state, which agrees with the experiment. The peak corresponding to 578 nm does not appear in the theoretical spectrum for ZnP, since the Q band is degenerate in this case.

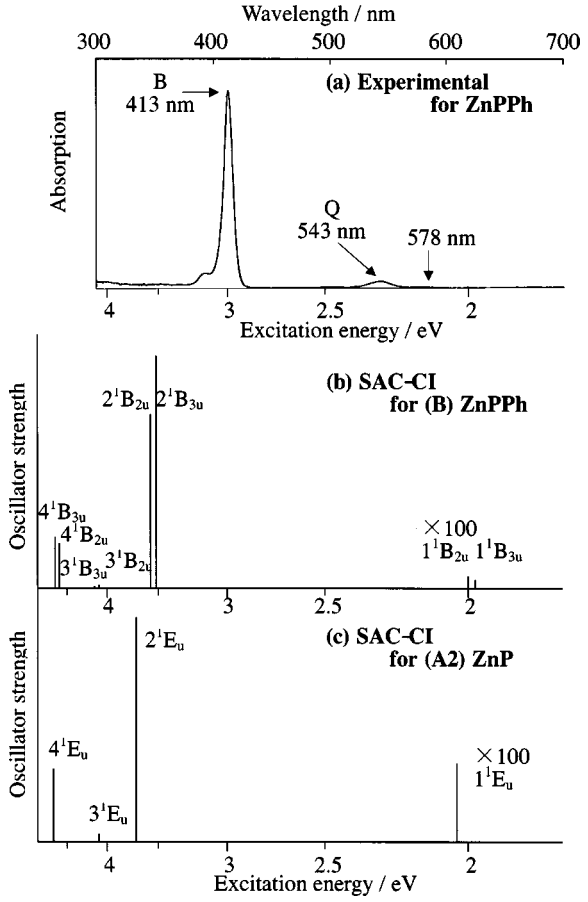

FIG. 9. (a) Experimental spectrum of zinc porphyrin monomer [2c], (b) the SAC-CI theoretical spectrum for (B) ZnPPh, and (c) the SAC-CI theoretical spectrum for (A2) ZnP.

The $2\,^1E_u$ state splits into the $2\,^1B_{2u}$ and $2\,^1B_{3u}$ states in ZnPPh. The oscillator strength of the $2\,^1B_{3u}$ state (2.30) is stronger than that of the $2\,^1B_{2u}$ state (1.72), since the transition dipole moment of the *x* axis with phenyl groups is stronger than that of the *y* axis. The magnetic circular dichroism (MCD)[19] of zinc porphin may indicate that the two peaks exist in around B band region. In ZnPPh, the B band shows a red-shift of 0.18 eV in the theoretical spectrum, in com-

TABLE II. Allowed excited states of zinc porphyrin monomer [(A1) ZnP] by the SAC-CI method.

	SAC-CI				SECI	Exptl.[a]
State	Main configurations[b] ($\|C\|>0.2$)	Nature	Excitation energy (eV)	Oscillator strength	Excitation energy (eV)	Exptl. eV (nm)
$1\,^1E_u$	$+0.684(1a_{1u}-5e_g)-0.655(5a_{2u}-5e_g)$	π-π^*	1.84	0.0129	2.56	2.28 (543)
$2\,^1E_u$	$+0.636(1a_{1u}-5e_g)+0.621(5a_{2u}-5e_g)$ $+0.296(4a_{2u}-5e_g)$	π-π^*	3.50	3.38	4.68	3.00 (413)
$3\,^1E_u$	$-0.904(2b_{2u}-5e_g)$	π-π^*	3.92	0.0827	5.39	
$4\,^1E_u$	$+0.860(4a_{2u}-5e_g)-0.230(5a_{2u}-5e_g)$	π-π^*	4.53	1.08	6.37	

[a]Reference 2(c).

[b]$1\,a_{1u}$ is HOMO(95), $5a_{2u}$ is next-HOMO(94), $5e_g$ is LUMO(96) or next-LUMO(97), $4a_{2u}$ is MO 90, $2b_{2u}$ is MO 93.

TABLE III. Allowed excited states of zinc porphyrin monomer [(B) ZnPPh] by the SAC-CI method.

	SAC-CI				SECI	Exptl.[a]
State	Main configurations[b] ($\|C\|>0.2$)	Nature	Excitation energy (eV)	Oscillator strength	Excitation energy (eV)	Exptl. eV (nm)
$1\ ^1B_{3u}$	$-0.671(13B_{1u}-12B_{2g})-0.666(4A_u-6B_{3g})$	π-π^*	1.98	8.56×10^{-4} (x)[c]	2.54	2.14 (578)
$1\ ^1B_{2u}$	$-0.678(13B_{1u}-6B_{3g})+0.662(4A_u-12B_{2g})$	π-π^*	2.00	1.18×10^{-3} (y)	2.55	2.28 (543)
$2\ ^1B_{3u}$	$+0.656(4A_u-6B_{3g})-0.628(13B_{1u}-12B_{2g})$ $-0.231(12B_{1u}-12B_{2g})$	π-π^*	3.52	2.30 (x)	4.52	3.00 (413)
$2\ ^1B_{2u}$	$+0.662(4A_u-12B_{2g})+0.611(13B_{1u}-6B_{3g})$ $+0.265(12B_{1u}-6B_{3g})$	π-π^*	3.57	1.72 (y)	4.60	
$3\ ^1B_{2u}$	$-0.647(2A_u-12B_{2g})+0.634(3A_u-12B_{2g})$	π-π^*	4.09	0.0351 (y)	5.36	
$3\ ^1B_{3u}$	$+0.640(2A_u-6B_{3g})-0.629(3A_u-6B_{3g})$	π-π^*	4.14	0.0199 (x)	5.34	
$4\ ^1B_{2u}$	$+0.865(12B_{1u}-6B_{3g})$	π-π^*	4.61	0.442 (y)	6.32	
$4\ ^1B_{3u}$	$+0.863(12B_{1u}-12B_{2g})$	π-π^*	4.67	0.508 (x)	6.31	

[a]Reference 2(c).
[b]$4A_u$ is HOMO(135), $13B_{1u}$ is next-HOMO(134), $3A_u$ is MO 133, $2A_u$ is MO 127, $12B_{1u}$ is MO 126, $6B_{3g}$ is LUMO(136), $12B_{2g}$ is next-LUMO(137).
[c]Parentheses show polarization.

parison with ZnP, and energy splitting occurs at each of the Q and B bands.

VI. EXCITED STATES OF THE MESO–MESO DIMER

Figure 10(a) shows the absorption spectrum for the meso–meso linked dimer [compound (a-2) in Fig. 1] in THF.[2(c)] Figure 10(b) shows the SAC-CI theoretical spectrum for Zn_2PMM. The theoretical and experimental spectra for the monomer ZnP (A1) are also shown for comparison. Table V summarizes the SAC-CI and SECI results for the optically allowed states of Zn_2PMM. The main configurations, characters, excitation energies and oscillator strengths are also shown.

Within the D_{2d} point group, there are two groups of optically allowed states, ^1E and $^1B_2$, and these two groups of excited states are classified as charge resonance and exciton states, respectively, for the following reason. The ^1E states represent the excitations from the localized MOs (186, 187) to the delocalized MOs (LUMO, 193) or from the delocalized MOs (HOMO, next-HOMO) to the localized MOs (191, 192), as seen in Fig. 4, while the $^1B_2$ states reflect the excitations from the localized MOs (186, 187) to the localized MOs (191, 192) or from the delocalized MOs (HOMO, next-HOMO) to the delocalized MOs (LUMO, 193).

A weak peak at 600 nm (2.07 eV) caused by the meso–meso dimerization is assigned to the $1\ ^1E$ state. The computed excitation energy is 1.76 eV. The main configuration of the $1\ ^1E$ state is not the excitation from the HOMO to the LUMO, but rather is characterized as the excitations within the eight orbitals: Four excited configurations in ^1E symmetry strongly interact with each other. The oscillator strength is similar to that in the monomer, as observed experimentally. Since the excitations are from the delocalized MOs to the localized MOs or vice versa, the transition dipole moment of this excitation is similar to that of the monomer. In the SECI results, the $1\ ^1E$ and $1\ ^1B_2$ states are almost degenerate. However, in the SAC-CI results, the $1\ ^1E$ state is redshifted by 0.3 eV, which shows the importance of electron correlations for reproducing the spectrum.

The Q band observed at 560 nm (2.21 eV) is assigned to the $1\ ^1B_2$ state calculated at 2.03 eV. The main configuration of the $1\ ^1B_2$ state is the excitation from HOMO to LUMO, which is the excitation within the eight orbitals. Since the MOs 192 and 190 originate from the LUMO of the monomer, the $1\ ^1B_2$ and $1\ ^1E$ states can be regarded as a pair of states which are split energetically by dimerization. The oscillator strength of the $1\ ^1B_2$ state (0.0886) is much larger than those of the $1\ ^1E$ state (7.04×10^{-3}) and monomer ZnP (0.0123). There are two reasons for this greater intensity. First, as expected from the molecular orbital shown in Fig. 4, the transition dipole moment between HOMO and LUMO is about twice as large as that of the monomer. Second, the

TABLE IV. Allowed excited states of zinc porphyrin monomer [(A2) ZnP] by the SAC-CI method.

	SAC-CI				SECI	Exptl.[a]
State	Main configurations[b] ($\|C\|>0.2$)	Nature	Excitation energy (eV)	Oscillator strength	Excitation energy (eV)	Exptl. eV (nm)
$1\ ^1E_u$	$-0.682(1a_{1u}-5e_g)+0.659(5a_{2u}-5e_g)$	π-π^*	2.03	0.0123	2.56	2.28 (543)
$2\ ^1E_u$	$+0.637(1a_{1u}-5e_g)+0.613(5a_{2u}-5e_g)$ $+0.306(4a_{2u}-5e_g)$	π-π^*	3.70	3.54	4.68	3.00 (413)
$3\ ^1E_u$	$+0.899(2b_{2u}-5e_g)$	π-π^*	4.09	0.121	5.39	
$4\ ^1E_u$	$-0.858(4a_{2u}-5e_g)+0.233(5a_{2u}-5e_g)$	π-π^*	4.70	1.14	6.37	

[a]Reference 2(c).
[b]$1\ a_{1u}$ is HOMO(95), $5a_{2u}$ is next-HOMO(94), $5e_g$ is LUMO(96) or next-LUMO(97), $4a_{2u}$ is MO 90, $2b_{2u}$ is MO 93.

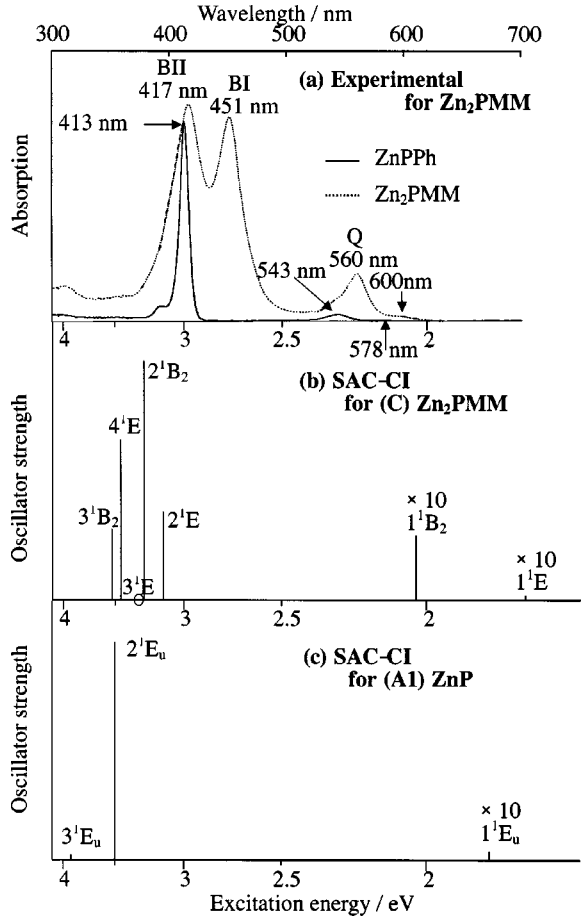

FIG. 10. (a) Experimental spectrum of zinc porphyrin monomer and meso-meso linked dimer [2c], (b) the SAC-CI theoretical spectrum for (C) Zn_2PMM, and (c) the SAC-CI theoretical spectrum for (A1) ZnP.

cancellation of the transition dipole moment by configuration interaction (CI) is not as complete as in the monomer, since the degeneracy and the near-degeneracy of the LUMO and the HOMO in the monomer are rather relaxed by the dimerization in Zn_2PMM.

The BI band is assigned to the $2\,^1E$ and $2\,^1B_2$ states calculated at 3.14 and 3.27 eV, respectively. The BII band is assigned to the $4\,^1E$ and $3\,^1B_2$ states calculated at 3.46 and 3.53 eV, respectively. This assignment helps to explain four peaks that appear in the B band region of the spectra for a similar system: Meso–meso linked strapped diporphyrin.[2(e)] The main configuration of the $2\,^1E$ and $2\,^1B_2$ states consists of the excitations from the HOMO, while the main configuration of the $4\,^1E$ and $3\,^1B_2$ states consists of the excitations from the next-HOMO. The $2\,^1E$ and $4\,^1E$ states, which respectively comprise the low-energy side of the BI and BII bands, have a charge resonance character.

The ^1E excited states could be viewed as due to the interactions of the two pairs of the four orbitals, where the first pair (Pair 1) and second pair (Pair 2) are composed of the excitations (189→192 and 187→190) and (188→192 and 187→193), respectively. These configurations in each pair correspond to the four-orbital excitations in the monomer, since MOs 188 and 189 originate from HOMO of the monomer, MO 187 from next-HOMO of the monomer, and MOs 190, 192, and 193 from LUMO of the monomer. The orbital energy gap of these excitations in Pair 1 is smaller than that in Pair 2. Pair 1 includes excitation from HOMO and to LUMO, while Pair 2 includes excitation from next-HOMO and to MO 193. In the $1\,^1E$ state, the signs of the coefficients for Pairs 1 and 2 are [189→192,187→190]=[+,−] and [188→192,187→193]=[+,−], respectively. These configuration interactions can be considered to be the Q band interactions, since the intensity of the $1\,^1E$ state is similar to that of the monomer Q band. The $2\,^1E$ state, which is assigned to the BI band, changes the sign of 189→192 (the sign in Pair 1 is [189→192,187→190]=[−,−] and that in Pair 2 is [188→192,187→193]=[+,−]), which means that Pair 1 becomes the *B* band interaction. Therefore, the intensity increases as large as that of the B band of the monomer. In the $3\,^1E$ state, both of the Pair 2 excitations 188→192 and 187→193 change sign (the sign in Pair 1 is [189→192,187→190]=[+,−] and that in Pair 2 is [188→192,187→193]=[−,+]), which again makes Pair 2

TABLE V. Allowed excited states of meso-meso-linked Zn-diporphyrin [(C) Zn_2PMM] by the SAC-CI method.

	SAC-CI				SECI	Exptl.[a]
State	Main configurations[b] ($\|C\|>0.2$)	Nature	Excitation energy (eV)	Oscillator strength	Excitation energy (eV)	Exptl. eV (nm)
$1\,^1E$	+0.539(189−192)−0.493(187−190)−0.433(187−193) +0.416(188−192)	π-π^*	1.76	7.04×10^{-3} (x,y)[c]	2.55	2.07 (600)
$1\,^1B_2$	+0.622(189−190)+0.444(188−193)+0.409(187−192) −0.409(186−191)	π-π^*	2.03	0.0886 (z)	2.53	2.21 (560)
$2\,^1E$	−0.743(189−192)−0.513(187−190)+0.220(188−192)	π-π^*	3.14	1.20 (x,y)	4.34	2.75 (451)
$2\,^1B_2$	+0.665(189−190)−0.473(187−192)+0.473(186−191)	π-π^*	3.27	3.26 (z)	4.14	2.75 (451)
$3\,^1E$	+0.635(187−193)−0.581(187−190)−0.304(188−192) +0.223(189−192)	π-π^*	3.28	1.86×10^{-3} (x,y)	4.93	
$4\,^1E$	+0.753(188−192)+0.520(187−193)	π-π^*	3.46	2.18 (x,y)	4.65	2.97 (417)
$3\,^1B_2$	+0.842(188−193)−0.284(189−190)−0.237(187−192) +0.237(186−191)	π-π^*	3.53	0.959 (z)	4.74	2.97 (417)

[a]Reference 2(c).
[b]In the *E* states, MOs 187 and 192 are written, since MOs 187 and 186, and MOs 192 and 191 are degenerate, respectively.
[c]Parentheses show polarization.

become the Q band interaction while Pairs 1 and 2 mix with different signs. This change reflects the transition intensity, as seen in Table V. In the 4 ^1E state, the sign for Pairs 1 and 2 are [189→192,187→190]=[+,+] and [188→192, 187→193]=[+,+], respectively, although the coefficient for 189→192 is very small. This mixing means that both Pairs 1 and 2 are in the B band interaction. This intensity is largest of the four ^1E states.

Similar to the ^1E state, two pairs of the four orbitals are considered in the $^1B_2$ excited states. The first pair (Pair 3) and the second pair (Pair 4) are composed of the excitations (189→190 and 187→192) and (188→193 and 186→191), respectively. Each pair has a four-orbital originating from HOMO, next-HOMO and degenerate LUMOs of the monomer. In the 1 $^1B_2$ state, the signs of the coefficients for Pairs 3 and 4 are [189→190,187→192]=[+,+] and [188→193,186→191]=[+,−], respectively. These interactions can be assumed to be the Q band interaction similar to the 1 ^1E states, since the intensity of the 1 $^1B_2$ state is weak, in comparison with the 2 or 3 $^1B_2$ states. In the 2 $^1B_2$ state, the signs for Pairs 3 and 4 are [189→190,187→192]=[+,−] and [188→193,186→191]=[−,+], respectively. Therefore, Pair 3 becomes the B band interaction and Pair 4 remains the Q band interaction. In the 3 $^1B_2$ state, Pair 3 remains the Q band interaction and Pair 4 becomes the B band interaction, since the signs of Pairs 3 and 4 are [189→190, 187→192]=[−,−] and [188→193,186→191]=[+,+], respectively. In the 3 $^1B_2$ state, the strong intensity is only due to the B band interaction in Pair 4, while in 2 $^1B_2$, the strong intensity originates not only from the B band interaction in Pair 3 but also from the Q band interaction in Pair 4, since the weights of the two excitations in Pair 4 are very different. Therefore, the intensity of the 2 $^1B_2$ state (3.26) is much stronger than that of the 3 $^1B_2$ state (0.959).

Kasha's exciton model[20] explains why the observed B bands of the dimer split into two peaks, as follows. The band with the lower energy (BI band) has a transition dipole moment along the *z* axis and the other band with the higher energy (BII band) has a transition dipole moment along the *x* or *y* axis. However, our computational results are different from this model, since the four peaks appear near the Soret band. The BI band has two components: The 2 ^1E state (*x* and *y* directions) and the 2 $^1B_2$ state (*z* direction). The BII band also has two components: The 3 $^1B_2$ state (*z*-direction) and the 4 ^1E state (*x* and *y* directions). As clearly seen in Fig. 4, the HOMO of the monomer gives the HOMO and next-HOMO of the dimer, while the LUMO of the monomer gives the LUMO and MO 193. This energy splitting causes the split B bands in the dimer, as can be seen from the main configurations of the corresponding states, 2 ^1E and 4 ^1E and 2 $^1B_2$ and 3 $^1B_2$.

VII. DOUBLY FUSED DIMER

Figure 11 shows the experimental absorption spectrum of the doubly fused dimer, Zn_2PDF (compound a-3 in Fig. 1), in THF.[2(d)] The absorption spectrum shows many peaks in the observed energy range and is significantly different from those of the meso–meso linked dimer, Zn_2PMM (compound a-2 in Fig. 1) and the monomer. We labeled these peaks 1–8,

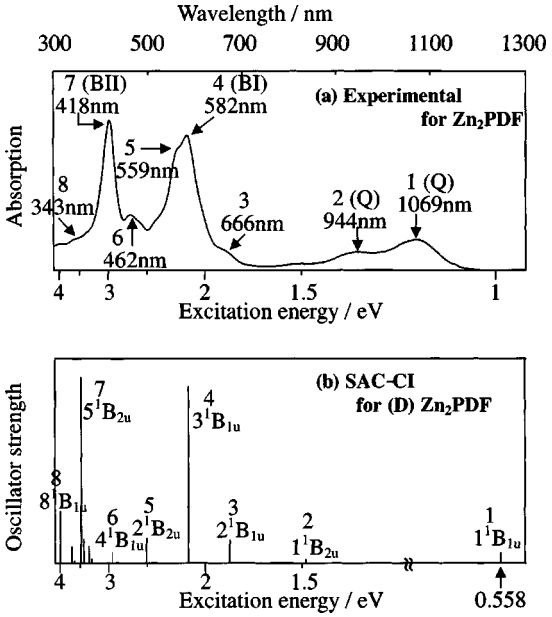

FIG. 11. (a) Experimental spectrum of doubly fused dimer [2d] and (b) the SAC-CI theoretical spectrum for (D) Zn_2PDF.

as indicated in Fig. 11. This complex spectrum indicates strong interaction between the monomer orbitals through π–π interactions at the co-planar meso–meso and β–β carbons. Figure 11 also shows the SAC-CI theoretical spectrum for Zn_2PDF, in comparison with the experimental spectrum for Zn_2PDF.

The SAC-CI spectrum of Zn_2PDF reproduced well the experimental one with regard to the peak positions and intensities, which allows us to give a reliable theoretical assignment. Table VI summarizes the SAC-CI and SECI theoretical results for the optically allowed states of Zn_2PDF. The main configurations, characters, excitation energies and oscillator strengths are given.

As the lowest excited state, we obtained 1 $^1B_{1u}$ state, which is assignable to peak 1 observed at 1.16 eV. The calculated excitation energy is 0.558 eV, which underestimates the experimental value by 0.6 eV. This discrepancy may be due to some approximations used in the present calculation. For example, the active space excludes many MOs higher than 1.3 Hartree, since the system is too large to perform an all-active calculation. The main configuration of the 1 $^1B_{1u}$ state is the excitation from the HOMO to LUMO. Since the HOMO–LUMO energy gap is so small (4.72 eV), this excitation energy is much smaller than those of ZnP and Zn_2PMM. A deformation of the HOMO and LUMO due to the dimerization affects the intensity of the peak, since the intensity cancellation caused by the configuration interaction no longer occurs.

Peak 2 observed at 1.31 eV is assigned to the 1 $^1B_{2u}$ state calculated at 1.49 eV. The main configuration is the excitation from MO 185 to LUMO and is characterized as the excitation within the eight orbitals, which corresponds to the four-orbital model in the monomer.

Peak 3 (1.86 eV) is assigned to the 2 $^1B_{1u}$ state calculated at 1.84 eV. The main configuration is represented by the two excitations from MO 183 to LUMO and from next-

TABLE VI. Allowed excited states of doubly fused Zn-diporphyrin [(D) Zn_2PDF] by the SAC-CI method.

	SAC-CI				SECI	Exptl.[a]
State	Main configurations ($\|C\|>0.2$)	Nature	Excitation energy (eV)	Oscillator strength	Excitation energy (eV)	Exptl. eV (nm)
$1\ ^1B_{1u}$	$+0.834(187-188)+0.326(186-189)-0.251(183-188)$	π-π^*	0.558	0.118 (z)[b]	1.79	1.16 (1069) [1][c]
$1\ ^1B_{2u}$	$-0.751(185-188)-0.479(187-190)-0.263(184-189)$	π-π^*	1.49	0.0404 (y)	2.47	1.31 (944) [2]
$2\ ^1B_{1u}$	$+0.677(183-188)+0.608(186-189)$	π-π^*	1.84	0.285 (z)	3.42	1.86 (666) [3]
$3\ ^1B_{1u}$	$+0.582(186-189)-0.577(183-188)-0.412(187-188)$	π-π^*	2.13	2.16 (z)	3.69	2.13 (582) [4]
$2\ ^1B_{2u}$	$+0.581(187-190)-0.502(186-191)-0.477(185-188)$	π-π^*	2.50	0.302 (y)	3.90	2.22 (559) [5]
$3\ ^1B_{2u}$	$-0.750(184-189)+0.398(187-190)+0.307(186-191)$	π-π^*	2.87	0.004 26 (y)	4.67	
$4\ ^1B_{1u}$	$+0.757(185-190)+0.311(182-189)-0.310(187-192)$ $-0.260(184-191)$	π-π^*	2.95	0.137 (z)	4.65	2.68 (462) [6]
$4\ ^1B_{2u}$	$-0.749(181-188)-0.403(176-188)-0.213(183-190)$	π-π^*	3.28	0.0503 (y)	5.06	
$5\ ^1B_{1u}$	$-0.549(187-192)+0.400(182-189)-0.381(178-188)$ $-0.363(185-190)+0.205(187-191,187-188)$	π-π^*	3.34	0.206 (z)	5.39	
$6\ ^1B_{1u}$	$+0.737(182-189)+0.410(187-192)$	π-π^*	3.44	0.295 (z)	5.66	
$5\ ^1B_{2u}$	$+0.622(186-191)+0.401(184-189)+0.329(187-190)$ $-0.240(185-188)+0.228(176-188)$	π-π^*	3.48	2.27 (y)	5.22	2.97 (418) [7]
$6\ ^1B_{2u}$	$+0.545(176-188)+0.535(183-190)-0.439(181-188)$	π-π^*	3.51	0.002 73 (y)	4.99	
$7\ ^1B_{1u}$	$+0.764(178-188)-0.276(187-192)-0.231(185-190)$ $-0.214(177-188)$	π-π^*	3.64	0.0309 (z)	5.10	
$7\ ^1B_{2u}$	$-0.661(183-190)+0.525(176-188)$	π-π^*	3.68	0.203 (y)	5.71	
$8\ ^1B_{1u}$	$+0.728(177-188)-0.260(184-191)+0.253(180-189)$ $-0.223(185-190)$	π-π^*	3.97	0.638 (z)	5.44	3.61 (343) [8]
$9\ ^1B_{1u}$	$+0.586(184-191)+0.543(180-189)+0.306(181-190)$ $-0.203(187-192)$	π-π^*	4.13	0.117 (z)	6.21	
$10\ ^1B_{1u}$	$+0.541(184-191)-0.520(180-189)+0.353(177-188)$ $-0.274(181-190)-0.258(187-192)$	π-π^*	4.24	0.001 81 (z)	5.91	
$8\ ^1B_{2u}$	$-0.617(185-192)-0.521(179-189)-0.244(186-191)$	π-π^*	4.43	0.204 (y)	6.22	

[a]Reference 2(d).
[b]Parentheses show polarization.
[c]The brackets show peak numbers.

HOMO to next-LUMO. The MO 183 originates from the ''fifth-orbital'' in the porphyrin monomer which is, in addition to Gouterman's four-orbital, involved in the excitation nature of the B band.[18] As seen from Fig. 7, the MO 183 of Zn_2PDF is localized at the inner four pyrrole rings. It is very remarkable that in the porphyrin systems the excitation outside of the four-orbital becomes the main configuration of such a low-lying state. In ZnP, this state corresponds to the $4\ ^1E_u$ state, with the computed excitation energy of 4.53 eV.

The BI band (peak 4) at 2.13 eV in the experiment is assigned to $3\ ^1B_{1u}$ state calculated at 2.13 eV. The main configuration consists of the excitations from next-HOMO to next-LUMO, MO 183 to LUMO, and HOMO to LUMO. Therefore, peaks 1 and 4 are in a similar relation to the Q and B bands in the monomer. In the $1\ ^1B_{1u}$ (peak 1) and $3\ ^1B_{1u}$ (peak 4) states, the sign of the coefficient is different, which causes a weak intensity in peak 1 and a strong intensity in peak 4, as in the Q and B bands of the monomer. The configuration interaction reduces the intensity of peak 1 and enhances that of peak 4.[5(a),(c)]

There is a shoulder on the blue-side (peak 5; 2.22 eV) of peak 4. This shoulder is assigned to $2\ ^1B_{2u}$ state calculated at 2.50 eV. The main configuration consists of the excitations within the eight-orbital corresponding to the Gouterman's four-orbital.

Peak 6 observed at 2.68 eV is assigned to $4\ ^1B_{1u}$ state calculated at 2.95 eV. The main configuration consists of the excitations including non-eight-orbital, from MO 185 to MO 190, from MO 182 to next-HOMO, and from HOMO to MO 192. The MOs 182 and 183 are localized at the inner four pyrrole rings, as seen in Fig. 7. The orbital energies of the MOs 182 and 183 are higher than those in ZnP and Zn_2PMM. The energy level of the MO 192 is lower than those in ZnP and Zn_2PMM by 0.7 eV. These changes are due to the dimerization. In the Soret band region of the monomer, there are no excitations to the orbitals higher than the next-LUMO, but in the dimer such excitations appear in the same energy region. The $5\ ^1B_{1u}$ and $6\ ^1B_{1u}$ states are calculated to be at 3.34 and 3.44 eV, respectively, and have the same main configurations with different mixing. The intensities of these states are around 0.2, which is large enough for observation. Probably, these two states would be hidden by the strong peak 7.

The BII band at 2.97 eV (peak 7) is assigned to the $5\ ^1B_{2u}$ state calculated at 3.48 eV. The main configuration consists of the excitations within the eight-orbital. In the B_{2u} irreducible representation, there are four excitations within the eight-orbital and hence four states appear due to the excitations (1, 2, 3 and $5\ ^1B_{2u}$ states). The $5\ ^1B_{2u}$ state is the highest state related to the eight-orbital excitations. The intensity of this state (2.27) is the greatest among the four states. The excitation energy (3.48 eV) of Zn_2PDF by SAC-CI is almost the same as those of ZnP (3.50 eV) and Zn_2PMM (3.46 eV). These states are related to the *B* band of the monomer.

On the blue-side of peak 7, several small peaks are ob-

served. One of them, peak 8 at 3.61 eV, can be assigned to the 8 $^1B_{1u}$ state calculated at 3.97 eV, since the computed intensity (0.638) is stronger than those of the other peaks and the energy difference between the 5 $^1B_{2u}$ and 8 $^1B_{1u}$ states (0.49 eV) is close to that between peaks 7 and 8 (0.63 eV). The main configuration of this state is the excitation from MO 177 to LUMO. The MO 177 has an orbital energy lower than that of the eight-orbital and its amplitude is localized on the outer four pyrrole rings, which is opposite the case from the MOs 182 or 183. The 6 $^1B_{2u}$ and 7 $^1B_{2u}$, and 7 $^1B_{1u}$ states consist of the excitations from outside the eight-orbital, but these states show weak intensities and would be hidden by peaks 7 and 8.

We now discuss the relationship between the molecular symmetry and the excited states, as clarified by the present calculations. In the $^1B_{1u}$ states, the main configurations are composed of the excitations from the unstabilized-occupied MOs (HOMO and next-HOMO) to the stabilized-unoccupied MOs (LUMO and next-LUMO), which cause a significant red-shift of the related peaks by about 0.9 eV compared to those in the monomer, ZnP. For example, peak 1 (1.16 eV) and peak 4 (2.13 eV) which, respectively, correspond to the Q and B bands in the monomer, are shifted to a lower energy by 0.9 eV, since the Q and B bands in ZnP are observed at around 2.0 and 3.0 eV, respectively.

In contrast to the $^1B_{1u}$ states, the main configurations of the $^1B_{2u}$ states consist of the excitations from the unstabilized-occupied MOs (HOMO and next-HOMO) to the unstabilized-unoccupied MOs (MOs 190 and 191) or from the stabilized-occupied MOs (MOs 184 and 185) to the stabilized-unoccupied MOs (LUMO and next-LUMO). Therefore, the energy change is smaller in the $^1B_{2u}$ states than in the $^1B_{1u}$ states. In the $^1B_2$ states, there are four states (1, 2, 3, and 5 $^1B_{2u}$) with excitation within the eight-orbital. Similar to the ^1E and $^1B_2$ states of the meso–meso dimer, four excitations are divided into two pairs. Pairs 1 and 2 consist of excitation (187→190 and 185→188) and (186→191 and 184→189), respectively. Each pair has a four-orbital originating from the four-orbital of the monomer. In the 1 $^1B_{2u}$ state, the signs of the coefficients for Pairs 1 and 2 are [187→190,185→188]=[−,−], [186→191, 184→189]=[+,−], respectively. Both Pairs 1 and 2 have the Q band interaction, since the 1 $^1B_{2u}$ state has weak intensity. In the 2 $^1B_{2u}$ state, the sign of the excitation 185→188 does not change ([187→190,185→188]=[+,−], [186→191, 184→189]=[−,+]). Therefore, Pair 1 in the 2 $^1B_{2u}$ state has the B band interaction. In the 3 $^1B_{2u}$ state, both Pairs 1 and 2 have the Q band interaction, since the signs of Pairs 1 and 2 are [187→190,185→188]=[+,+], [186→191,184→189]=[+,−], respectively. The 5 $^1B_{2u}$ state, which has strong intensity (2.27), is composed of the two B band interactions, since the signs of Pairs 1 and 2 are [187→190,185→188]=[+,−], [186→191,184→189]=[+,+], respectively. In the 1 $^1B_{2u}$ and 2 $^1B_{2u}$ states, the coefficients of Pair 1 are larger than those of Pair 2, while the coefficients of Pair 1 are smaller than those of Pair 2 in the 3 $^1B_{2u}$ and 5 $^1B_{2u}$ states. The excitation energies of the 1 $^1B_{2u}$ and 2 $^1B_{2u}$ states are lower than those of the 3 $^1B_{2u}$ and 5 $^1B_{2u}$ states, since the orbital energy gaps in Pair 1 are smaller than those in Pair 2.

VIII. CONCLUSION

The SAC-CI calculations were carried out for the excited state of Zn porphyrin dimers; meso–meso connected Zn_2PMM and doubly fused Zn_2PDF. Calculations were also made for Zn porphyrin monomer for comparison. The resulting theoretical spectra successfully reproduced the experimental ones, being well enough to enable reliable assignments. The SAC-CI calculations clarified the electronic structures of the excited states of these dimers, which are much more complex than those of the monomer.

For the monomer, calculation (B) for ZnPPh reproduced the weak peaks at 578 and 543 nm and also the B band seen in the experimental spectrum. The substituents in ZnPPh cause a splitting of the Q band, due to a reduction of molecular symmetry.

Calculation (C) for Zn_2PMM reproduced the Q bands at 600 and 560 nm and the BI and BII bands. The dimerization cause an energy gap between the HOMO and the next-HOMO and also between the LUMO and the MO 193, which cause a splitting of the Soret band into BI and BII bands. All of the peaks of the Q, BI, and BII bands consist of a pair of states; ^1E and $^1B_2$ states. The splitting seen in the dimer spectrum is caused by the interaction between HOMOs and between LUMOs of the monomer, which is clearly seen in the main configuration. Kasha's exciton rule does not necessary hold, since each of the BI and BII bands consists of two excited states.

The SAC-CI calculation (D) for Zn_2PDF successfully reproduced the experimental spectrum, with many peaks in the observed range, and a reliable theoretical assignment was possible for all of the peaks. The dimerization in Zn_2PDF significantly unstabilizes/stabilizes the HOMO–LUMO levels, which stabilizes the HOMO→LUMO excitation. As a result, the Q bands are significantly red-shifted and have a relatively strong intensity. The stabilization of LUMO levels causes a red-shift of high-lying excited states, which can be assigned to the 2, 5, and 6 $^1B_{1u}$ and 4 $^1B_{2u}$ states. Due to the symmetry of the molecule, the $^1B_{1u}$ excited configurations can be characterized as the excitations from the unstablilized occupied MOs to the stabilized unoccupied MOs. Therefore, a significant red-shift is observed in the spectrum. The Q and B bands in the $^1B_{1u}$ state appear at 1.16 and 2.13 eV, respectively. The BI band has a transition dipole moment along the *z* axis, while the BII band has a transition dipole moment along the *x* or *y* axis. The BI band is red-shifted more than that of Zn_2PMM, since the HOMO–LUMO energy gap is much smaller than that in Zn_2PMM.

ACKNOWLEDGMENTS

This study was supported by the Grant for Creative Scientific Research from the Ministry of Education, Science, Culture, and Sports of Japan, and partially by the grant from Matsuo Foundation.

[1] A. K. Burrell, D. L. Officer, P. G. Plieger, and D. C. W. Reid, Chem. Rev. **101**, 2751 (2001).

[2] (a) T. Ogawa, Y. Nishimoto, N. Yoshida, N. Ono, and A. Osuka, Angew. Chem. Int. Ed. Engl. **38**, 176 (1999); (b) A. Tsuda, A. Nakano, H. Furuta, H. Yamochi, and A. Osuka, *ibid.* **39**, 558 (2000); (c) N. Aratani, A. Osuka,

Y. H. Kim, D. H. Jeong, and D. Kim, *ibid.* **39**, 1458 (2000); (d) A. Tsuda, H. Furuta, and A. Osuka, *ibid.* **39**, 2549 (2000); (e) N. Yoshida and A. Osuka, Org. Lett. **2**, 2963 (2000); (f) N. Yoshida, N. Aratani, and A. Osuka, Chem. Commun. (Cambridge) **2000**, 197 (2000); (g) A. Tsuda, H. Furuta, and A. Osuka, J. Am. Chem. Soc. **123**, 10304 (2001); (h) H. S. Cho, N. W. Song, Y. H. Kim, S. C. Jeoung, S. Hahn, D. Kim, S. K. Kim, N. Yoshida, and A. Osuka, J. Phys. Chem. A **104**, 3287 (2000); (i) H. S. Cho, D. H. Jeong, M. C. Yoon *et al.*, *ibid.* **105**, 4200 (2001).

[3] M. R. Wasielewski, Chem. Rev. **92**, 435 (1992); D. Gust, T. A. Moore, and L. Moore, Acc. Chem. Res. **34**, 40 (2001).

[4] R. E. Martin and F. Diederich, Angew. Chem. Int. Ed. Engl. **38**, 1350 (1999).

[5] (a) J. Hasegawa, M. Hada, M. Nonoguchi, and H. Nakatsuji, Chem. Phys. Lett. **250**, 159 (1996); (b) H. Nakatsuji, J. Hasegawa, H. Ueda, and M. Hada, *ibid.* **250**, 379 (1996); (c) K. Toyota, J. Hasegawa, and H. Nakatsuji, *ibid.* **250**, 437 (1996); (d) H. Nakatsuji, Y. Tokita, J. Hasegawa, and M. Hada, *ibid.* **256**, 220 (1996); (e) H. Nakatsuji, J. Hasegawa, and M. Hada, J. Chem. Phys. **104**, 2321 (1996); (f) K. Toyota, J. Hasegawa, and H. Nakatsuji, J. Phys. Chem. A **101**, 446 (1997); (g) Y. Tokita and H. Nakatsuji, J. Phys. Chem. B **101**, 3281 (1997); (h) Y. Tokita, J. Hasegawa, and H. Nakatsuji, J. Phys. Chem. A **102**, 1843 (1998); (i) T. Miyahara, Y. Tokita, and H. Nakatsuji, J. Phys. Chem. B **105**, 7341 (2001).

[6] H. Nakatsuji and K. Hirao, J. Chem. Phys. **68**, 2053 (1978).

[7] H. Nakatsuji, Chem. Phys. Lett. **59**, 362 (1978); H. Nakatsuji, *ibid.* **67**, 329, 334 (1979).

[8] H. Nakatsuji, *Computational Chemistry—Reviews of Recent Trends*, edited by J. Leszczynski (World Scientific, Singapore, 1997), Vol. 2; SAC-CI Method: Theoretical Aspects and Some Recent Topics.

[9] H. Nakatsuji, Acta Chim. Hung. **129**, 719 (1992).

[10] P. Hohenberg and W. Kohn, Phys. Rev. **136**, B864 (1964); W. Kohn and L. J. Sham, Phys. Rev. A **140**, 1133 (1965); R. G. Parr and W. Yang, *Density-functional theory of atoms and molecules* (Oxford University Press, Oxford, 1989).

[11] C. Lee, W. Yang, and R. G. Parr, Phys. Rev. B **37**, 785 (1988); A. D. Becke, J. Chem. Phys. **98**, 5648 (1993).

[12] S. Huzinaga, J. Andzelm, M. Klobukowski, E. Radzio-Andzelm, E. Sakai, and H. Takewaki, *Gaussian basis set for molecular calculation* (Elsevier, New York, 1984).

[13] S. Huzinaga, J. Chem. Phys. **42**, 1293 (1965).

[14] M. J. Frisch, G. W. Trucks, H. B. Schlegel *et al.*, GAUSSAN 98, Gaussian, Inc., Pittsburgh, PA (1998).

[15] H. Nakatsuji, M. Hada, M. Ehara, J. Hasegawa, T. Nakajima, H. Nakai, O. Kitao, and K. Toyota, SAC/SAC-CI program system (SAC-CI96) for calculating ground, excited ionized, and electron-attached states and singlet to septet spin multiplicities (1998).

[16] H. Nakatsuji, Chem. Phys. **75**, 425 (1983).

[17] M. Gouterman, *The porphyrins*, edited by D. Dolphin (Academic, New York, 1977), Vol. III.

[18] Y. Yamamoto, T. Noro, and K. Ohno, Int. J. Quantum Chem. **42**, 1563 (1992).

[19] J. D. Keegan, A. M. Stolzenberg, Y.-C. Lu, R. E. Linder, G. Barth, A. Moscowitz, E. Bunnenberg, and C. Djerassi, J. Am. Chem. Soc. **104**, 4305 (1982); H. Sekino and H. Kobayashi, J. Chem. Phys. **86**, 5045 (1987).

[20] H. L. Anderson, Inorg. Chem. **33**, 972 (1994); K. Susumu, T. Shimidzu, K. Tanaka, and H. Segawa, Tetrahedron Lett. **37**, 8399 (1996).